

Yang, K-H., Zornberg, J.G., Liu, C-N. and Lin, H-D. (2012). "Backfill Stress and Strain Information within a Centrifuge Geosynthetic-Reinforced Slope under Working Stress and Large Soil Strain Conditions," Proceedings of the ASCE Geo-Congress 2012, Oakland, California, 25-29 March 2012, Geotechnical Special Publication no. 225, pp.461-470.

## **Backfill Stress and Strain Information within a Centrifuge Geosynthetic-Reinforced Slope Model under Working Stress and Large Soil Strain Conditions**

Kuo-Hsin Yang<sup>1</sup>, Jorge G. Zornberg<sup>2</sup>, Chia-Nan Liu<sup>3</sup>, Horn-Da Lin<sup>4</sup>

<sup>1</sup>Department of Construction Engineering, National Taiwan University of Science and Technology, email:khy@mail.ntust.edu.tw

<sup>2</sup> Department of Civil, Architectural and Environmental Engineering, The University of Texas at Austin, email: zornberg@mail.utexas.edu

<sup>3</sup> Department of Civil Engineering, National Chi-Nan University, email: cnliu@ncnu.edu.tw

<sup>4</sup>Department of Construction Engineering, National Taiwan University of Science and Technology, email:hdlin@mail.ntust.edu.tw

### **ABSTRACT**

Numerical methods combined with a centrifuge test are used to investigate the mobilization of backfill stress and strain within a geosynthetic-reinforced soil (GRS) slope under working stress and large soil strain conditions. System stability indicated by the factor of safety ( $FS$ ) of the GRS slope is calculated using limit equilibrium analysis. The stress and strain information under various soil stress states is evaluated using a finite element model with a soil constitutive model capable of modeling soil softening behavior. The numerical models are verified by data from a centrifuge GRS slope model. Numerical results indicate that soil stress mobilization can be described with soil stress level  $S$ , which is defined as the ratio of current stress status to peak failure criteria. As loading increases, backfill stresses develop and propagate along the potential failure surface. Mobilization of soil stress was non-uniform along the failure surface. Immediately after the stress level reaches peak ( $S=1$ ), strength softening initiates at the top and toe of the slope at approximately  $FS=1.2$ . The slope settlement rate and reinforcement tensile load significantly increase when soil softening begins. The softening occurs randomly and irregularly along the failure surface and the formation of soil softening band completes at approximately  $FS=1.1$ . The failure surface corresponds to the locus of intense soil strains and the maximum tensile loads at each reinforcement layer.

*Key Words* : Geosynthetics reinforced soil structures, Stress distribution, and Finite element analysis

## INTRODUCTION

The backfill stress and strain information within retaining earth structures is an important factor to understand the basis of design (*e.g.*, examine the design methods in current guidelines) and answer several current design arguments (*e.g.*, select soil peak or residual shear strength properties for design) (Leshchinsky, 2001; Zornberg, 2002; Zornberg and Leshchinsky, 2001). However, the backfill stress and strain information has not been extensively studied yet. That is because this information is often not directly accessible through most of current physical or numerical methods. Physical methods like *in-situ* monitoring and full-scale tests typically use pressure cells to measure soil pressure. However, adjusting pressure cells in the orientation of interest (*e.g.*, soil stress along the failure surface) after installation is difficult. Small-scale models used in centrifuge tests also raise concerns that intrusive instrumentation may disturb the development of soil stresses. Numerical simulations provide limited useful data on soil stress and strain. For example, although finite element method satisfactorily models conservatively designed GRS structures under working stress conditions, it is inadequate for predicting the behavior of GRS structures under large deformation conditions. This problem arises because most soil constitutive models do not consider the post-peak behavior of soil. This is a crucial problem when evaluating soil stresses under large soil strain conditions, especially in comparatively flexible structures such as GRS structures. Numerical accuracy and stability are particularly important at the post-peak region of soil.

This observation has prompted the current study to examine the backfill stress and strain information within GRS structures. The objective is to characterize the distribution and development of backfill stresses and strains within a GRS slope by combining several methods. A limit equilibrium analysis is used to calculate the factor of safety of the GRS slope. A finite element model with a soil constitutive model capable of modeling soil softening behavior is used to study the mobilization of soil stresses and strains under various soil stress states. The proposed numerical models are verified using data from a centrifuge test on a GRS slope. The stress and strain data obtained by the numerical simulations is useful for interpreting the behavior of GRS structures and offers valuable insights into the design of GRS structures.

## MODELING OF A GRS SLOPE

### Centrifuge Test

A series of centrifuge tests on GRS reinforced slopes was conducted by Arriaga (2003) to investigate the response of GRS slopes to various design factors, *e.g.*, backfill relative density, slope angle, reinforcement vertical spacing and reinforcement type. One centrifuge test (slope model M1) was selected for numerical

simulation and verification. The dimensions and reinforcement layout of slope M1 are illustrated in Fig. 1. Monterey No. 30 sand with a target relative density of  $D_r=70\%$  was used as the backfill and foundation soil. For this relative density, the peak friction angle was  $\phi_{tc}=36.7^\circ$  under triaxial compression conditions and  $\phi_{ps}=42^\circ$  under plane strain conditions. The unit weight of the backfill was  $16.0 \text{ kN/m}^3$ . The reinforcement used in the centrifuge study was a commercially available nonwoven geotextile. The average unconfined tensile strength from wide-width tensile tests was  $0.03 \text{ kN/m}$ . The confined tensile strength value, obtained from back-calculation at failure in the centrifuge slope models, was  $0.124 \text{ kN/m}$  (Arriaga, 2003). Each loading stage was applied in  $5g$  increments and the total  $g$ -level  $N_g$  required to fail the slope was  $50g$  at which the slope model is equivalent to  $11.4\text{m}$  high in prototype. Slope failure was determined by a sudden large increase in settlement measured by a linear variable differential transformer (LVDT) located at  $38.1\text{mm}$  from the front crest of the slope, as indicated in Fig. 1. The location of failure surface of slope model M1 was identified from the observed tear (rupture) in each layer of the reinforcement, which is plotted as the blue triangular symbols in Fig. 2.

### Limit Equilibrium Analysis

Limit equilibrium analyses were performed by Spencer's method with circular surfaces to calculate the factor of safety and to locate the failure surfaces on the GRS slope. The plane strain friction angle  $\phi_{ps}=42^\circ$  was used to characterize the shear strength of the Monterey No. 30 sand. The centrifugal force was simulated by increasing the unit weight of backfill  $N$  times corresponding to the target  $g$ -level.

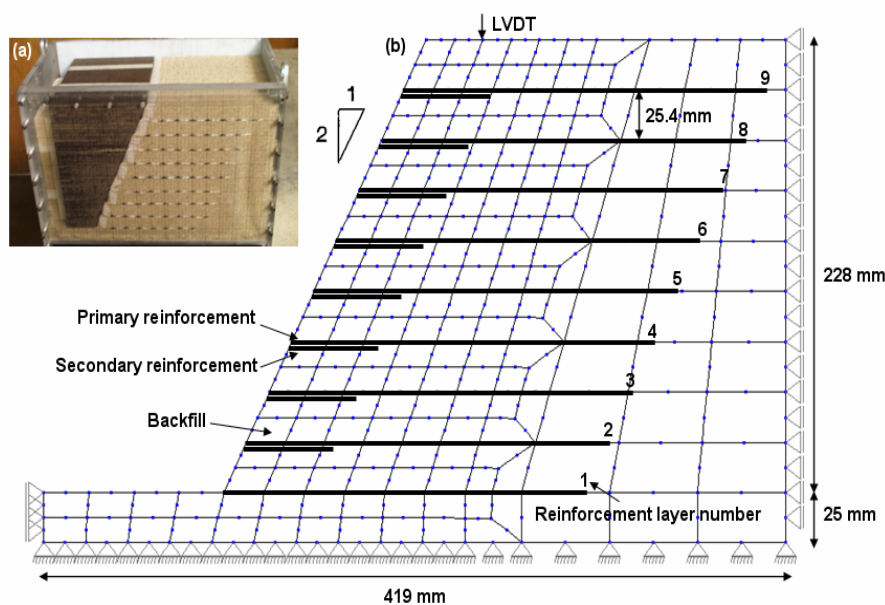


Figure 1. Dimensions and layout of slope model M1

The location of the failure surface identified from the limit equilibrium analysis, the dash line as shown in Fig. 2, was compared to that found from the centrifuge test. In this study, the back-calculated ultimate confined tensile strength of reinforcement was used to estimate the *FS* of the centrifuge model as the *g*-level increases. Figure 3 shows the relationships between *FS* and *g*-level for the slope model M1. The calculated *FS* generally decreases as *g*-level increases, which suggests that system stability decreases as loading increases. Unlike the recommended use of allowable tensile strength in the conventional analysis, the limit equilibrium analyses in this study did not consider reduction factors due to installation damage, creep or degradation (*i.e.*, all reduction factors were 1.0). Reduction factors were excluded because the centrifuge model was carefully constructed to ensure that no installation damage occurred, and the test duration was kept relatively short so that no long-term behavior such as creep or degradation would occur.

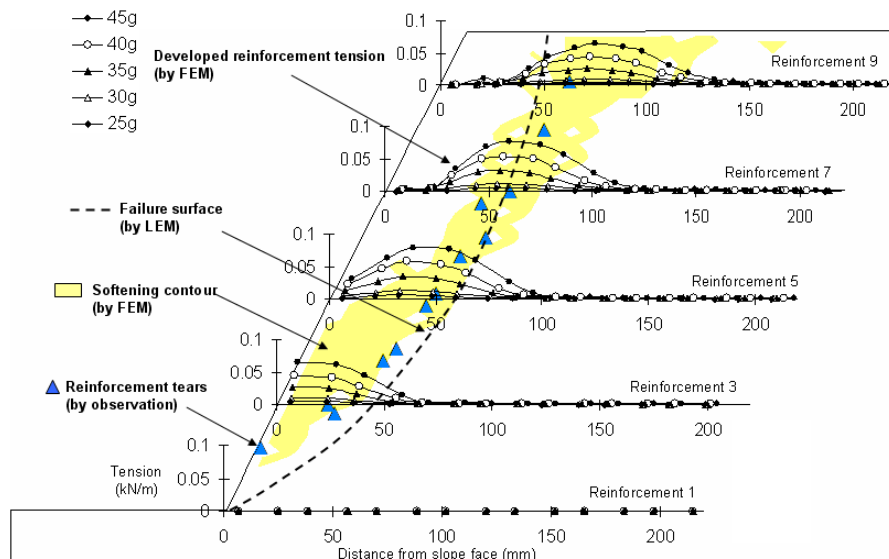


Figure 2. Comparison of failure surface locations in slope model M1

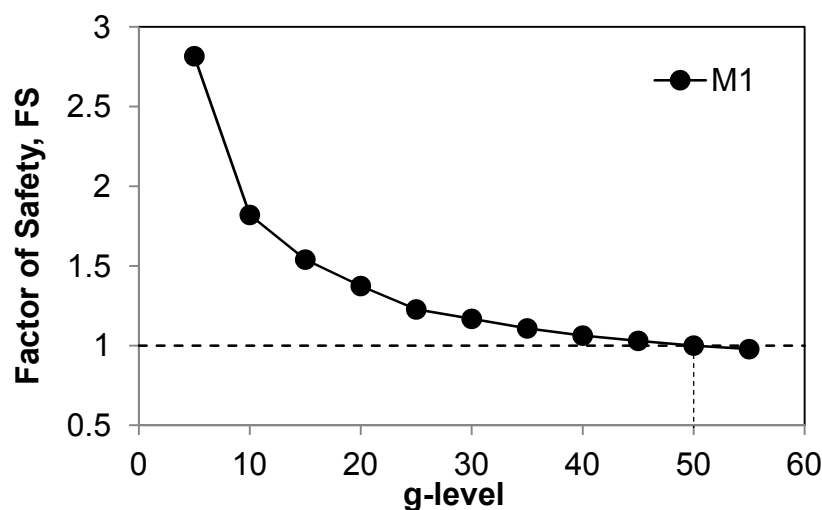


Figure 3. Calculated factor of safety vs. *g*-level for slope model M1

### Finite Element Simulation

Finite element modeling was carried out using the in-house developed finite element program, Nonlinear Analysis of Geotechnical Program (ANLOG). ANLOG is coded in FORTRAN. Figure 1 shows the initial settings of the slope model M1. Standard boundaries were imposed to simulate confinement at the edges of aluminum centrifuge box. Mesh updating was used to account for large model deformations. The centrifugal force of the centrifuge was simulated by increasing the body force on each element. The Lade-Kim elastoplastic constitutive model (Lade and Jakobsen, 2002) combined with a modified soil softening model (Yang, 2009) was implemented in program ANLOG to model soil behavior at various stress states. The soil softening behavior was numerically governed by the yield surface contraction. As soil strength changes from hardening (pre-peak) to softening (post-peak), the yield surface changes from expansion to contraction. Figure 4 shows the comparison of predicted soil stress-strain relationships and those measured from triaxial compression tests. Table 1 summarizes the calibrated parameter values for Monterey No. 30 sand. The softening parameters in Table 1 correlate with confining pressures and can be regressed as linear functions of confining pressures.

Reinforcement layers were simulated using bar elements with only one degree of freedom in the horizontal direction. A nonlinear elastic reinforcement model based on a second order polynomial was used to equate tensile load to tensile strain (Karpurapu and Bathurst, 1995). The reinforcement model parameters were calibrated using the load-strain data of reinforcement under confined conditions. This confined load-strain data is assumed to exhibit the similar trend observed in wide-width tensile test under unconfined conditions except that the unconfined curve is multiplied by the

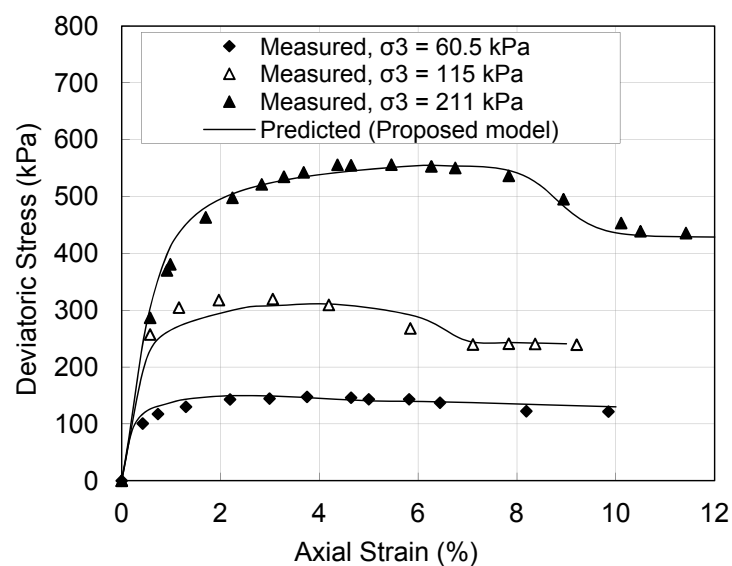


Figure 4. Comparison of measured and predicted stress-strain response

ratio of ultimate confined tensile strength to ultimate unconfined tensile strength. The interface element was not adopted in the numerical model. The approach used in the numerical modeling was supported by the visual observation that reinforcement specimens ruptured rather than failed due to pullout in the centrifuge tests.

The simulation results were compared with centrifuge results to verify the accuracy of the proposed finite element model. Figure 2 shows the comparison of the location of measured and predicted failure surfaces. Figure 5 shows the comparison of measured and predicted settlement at the front crest of the slope model M1. The verification also was carried out to compare the slope deformation pattern and the reinforcement displacement along each layer but not shown here. All predicted and measured results were judged to be in satisfactory agreement. The readers are referred to Yang (2009) for more details of the finite element model simulation and verification.

**Table 1. Backfill properties for Monterey No. 30 sand**

| Model component        | Parameter                     | Input Value                      |
|------------------------|-------------------------------|----------------------------------|
| Unit weight            | $\gamma$ (kN/m <sup>3</sup> ) | 16.0                             |
| Elastic model          | $M, \lambda, \nu$             | 705, 0.257, 0.35                 |
| Failure criterion      | $m, \eta_1, a'$               | 0.0214, 29.3, 0                  |
| Plastic potential      | $\psi_2, \mu$                 | -8.51, 2.2                       |
| Yield criterion        | $h, \alpha$                   | 0.67, 0.2                        |
| Hardening law          | $C, p$                        | $5.07 \times 10^{-5}, 1.9$       |
| Modified softening law | $a$                           | $a = 0.0076\sigma_3 + 0.27$      |
|                        | $b$                           | $b = -0.737\sigma_3 + 209.8$     |
|                        | $f_{pr}''$                    | $f_{pr}'' = 0.30\sigma_3 + 20.9$ |

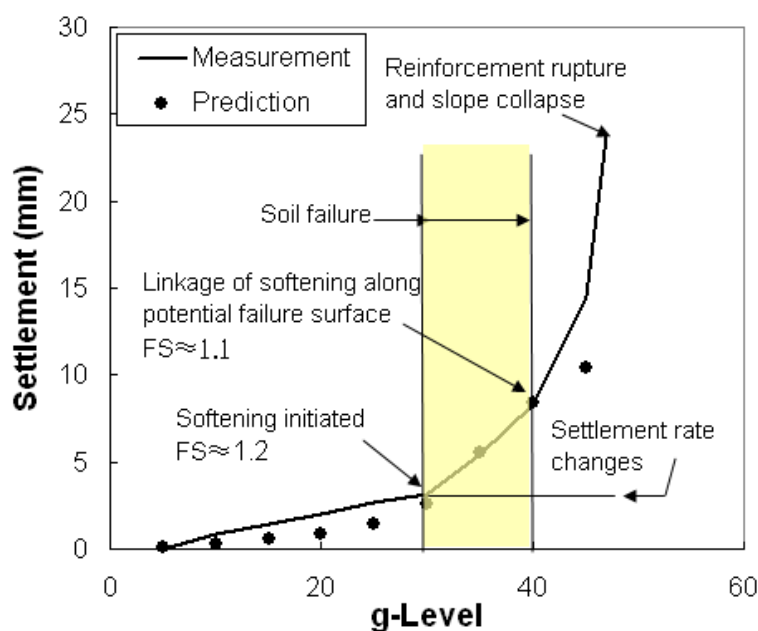


**Figure 5. Settlement at front crest of centrifuge slope model M1 with g-level**

## RESULTS AND DISCUSSION

### Soil Stress Information

After the finite element model was verified, the soil stress and strain information can be obtained. The mobilization of soil stress can be described using soil stress level  $S$ , which is defined as the ratio of current stress status to peak failure criteria. The value of  $S$  is low when the current stress state is far away from peak strength and  $S$  equals to 1.0 when the current stress state reaches peak strength.  $S$  is large than 1.0 when soil stress state crosses peak strength and reaches the strength softening region. In the soil softening region, the range of  $S$  is defined from 1.0 to 2.0. The results of  $S$  varying with various g-level are shown in Figs. 6.

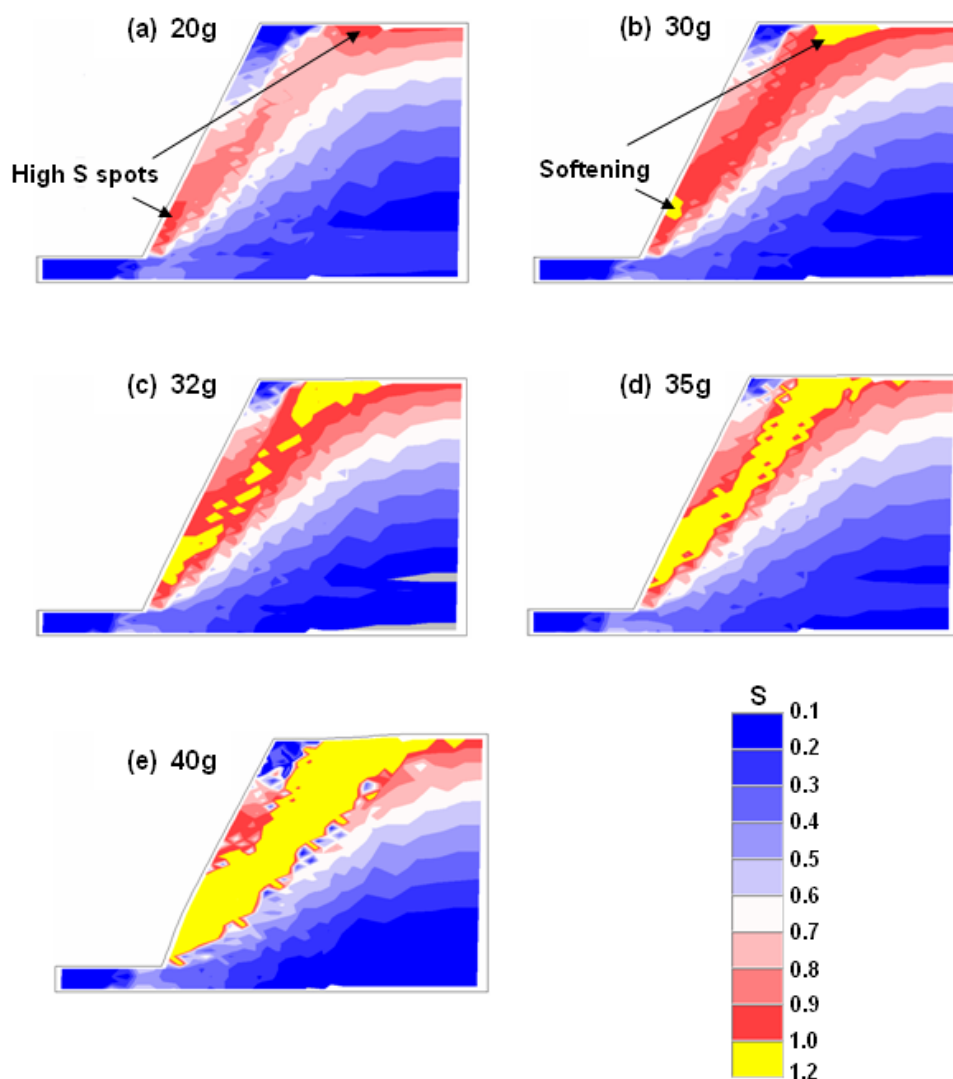


**Figure 6. Stress level distribution and development for slope model M1: (a) 20g, FS=1.37; (b)30g, FS=1.16; (c) 32g, FS=1.13; (d) 35g, FS=1.10; (e) 40g, FS=1.06**

In Figs. 6, the backfill stress that develops with increased load propagates along the potential failure surface. Two high stress level areas reach 0.9 at the top and toe of

the slope (Fig. 6a). Immediately after the stress level reaches peak ( $S=1$ ), strength softening occurs at the top and toe of the slope at approximately 30g ( $FS=1.16$ ) (Fig. 6b). The softening occurs randomly and irregularly along the failure surface (Fig. 6c) and then forms a clear softening band (Fig. 6d). The completed linkage of soil softening band throughout the entire potential failure surface occurs at approximately 40g ( $FS=1.06$ ) (Fig. 6e). The observed formation of failure surfaces observed in this study is consistent with several studies of the shear behavior of sand in the context of shear band development (*e.g.*, Suzuki and Yamada, 2006; Yoshida and Tatsuoka, 1997; Yoshida *et al.*, 1993).

The observed results for  $S$  have two design implications. First, Figs. 6 show that the mobilization of  $S$  is clearly non-uniform along the failure surface. This observation contradicts current assumptions regarding the internal stability of GRS structures. That is, current design methods based on earth pressure theory or limit equilibrium method assume that the soil shear strength along the failure surface mobilizes equally and reaches peak shear strength simultaneously. Second, the current design requires  $FS \geq 1.3$  to achieve global stability in a reinforced slope. In contrast, Fig. 6 shows soil softening has not initiated at  $FS \geq 1.3$ . Therefore, the soil stress state is still below its peak shear strength at  $FS \geq 1.3$ . This suggests  $FS \geq 1.3$  is a good criterion for ensuring the serviceability of slopes (*i.e.*, the developed soil stress state is under work stress conditions).

Another important observation in this study is the increase of settlement rate, indicated in Fig. 5, corresponds to the status of soil-softening developed along the failure surface. The soil softening is initiated in some soil elements around 30g in the numerical simulation and the linkage of softening zone along failure surface is completed around 40g. During this period, the settlement rate of the GRS slope shows a significant increase. Similar observations were reported by Bathurst (1993) and Karpurapu and Bathurst (1995) in tests of two instrumented large-scaled GRS retaining walls in the Royal Military College (RMC) retaining wall test facility. They reported that the rate of facial displacement increased significantly at soil failure.

Moreover, it is observed from the numerical simulation that the reinforcement tension does not be mobilized significantly until soil softening occurs. As shown in Fig. 2, the mobilization of reinforcement tension becomes noticeable only after the g-level reached 30g when the soil softening starts to be initiated. The significant mobilization of reinforcement tensile load after soil softening indicates load transfer from soils to reinforcements. At soil post-peak stage, the reinforcement tensile loads have to be mobilized significantly in order to offset the increasing centrifuge loading and, meanwhile, the decreasing soil strength (dropping from peak to residual strength). Although the mobilization of reinforcement tensile loads at soil post-peak

stage maintains system stability, incremental system deformation increases rapidly (Fig 5). Depending on the tensile strength of reinforcement, system failure ( $FS=1.0$ ) may occur after only a few loading increments.

### Soil Strain Information

Examining the soil strain information obtained from the numerical simulation found the failure surface corresponds to the locus of intense soil strains in the horizontal, vertical and shear directions (Figs. 7) and the locus of the peak reinforcement strains at each layer (see Fig. 2). This clearly indicates significant deformation happens along the failure surface. Due to the dilatancy of frictional materials, the soil horizontal strain along the failure surface appears in tension, as the negative value of strain indicated in Fig 7a. It appears that the final collapse of the GRS slope (sliding of active soil wedge) is driven by a significant deformation along the failure surface. When the system deformation-induced soil strains reach certain intensity, the mobilized reinforcement tensile loads reach their ultimate strength (reinforcement breakage occurs) and cause the final collapse of the slope.

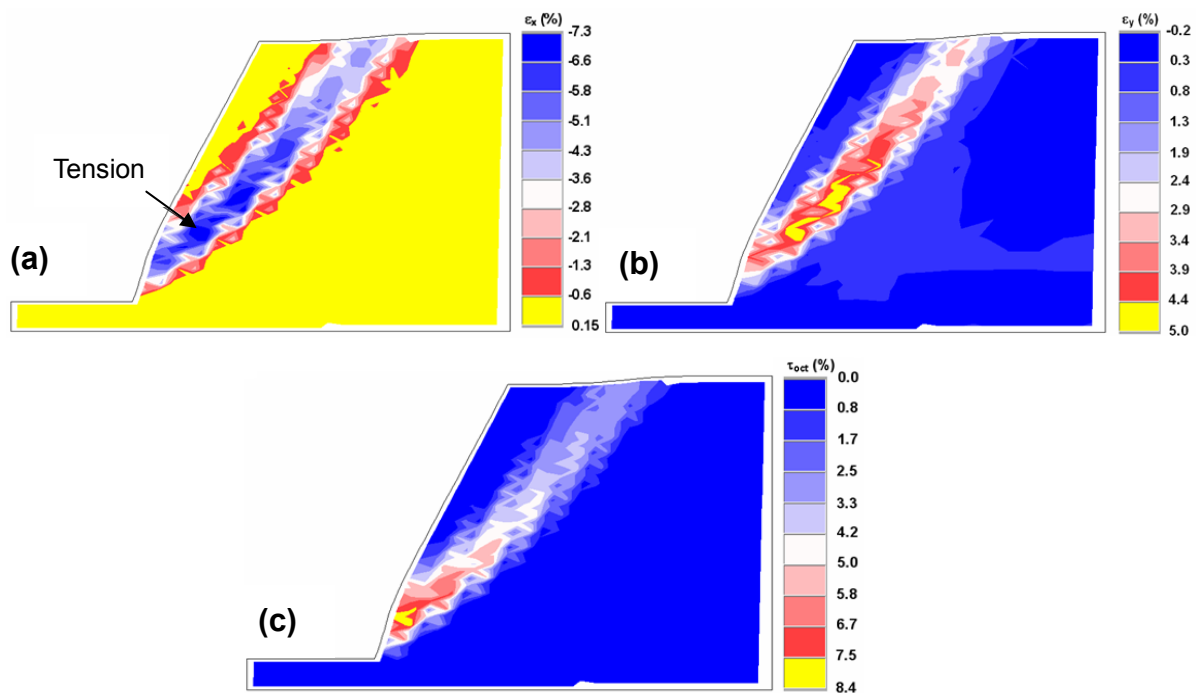


**Figure 7. Developed soil strain for slope model M1: (a) horizontal strain  $\epsilon_x$ ; (b) vertical strain  $\epsilon_y$ ; (c) shear strain in octahedral plane  $\tau_{oct}$**

### SUMMARY

In this paper, numerical studies of a centrifuge slope model were applied to investigate the mobilization of backfill stress and strain within GRS structures under various soil stress states. The results indicate, as the loading increases, the soil stress is mobilized and propagated non-uniformly along the potential failure surface. The

soil stress level reaches one and strength softening is initiated immediately at top and toe of slope. Before soil softening occurs, the mobilization of reinforcement tensile loads and system deformation does not increase significantly. The softening, then, occurs randomly and irregularly along failure surface and a clear softening band forms. After the completed linkage of soil softening band through the entire potential failure surface, the system stability mainly sustains by the mobilized reinforcement tensile loads. The system reaches failure soon by few loading increments depending on reinforcement tensile strength. It is also observed that the failure surface corresponds to the locus of intense soil strains and the maximum tensile loads at each reinforcement layer, which clearly indicates significant deformation happens along the failure surface.

## REFERENCES

- Arriaga, F. (2003). “Responses of geosynthetic reinforced structures under working stress and failure conditions”, Ph.D. dissertation, Department of Civil, Architectural, and Environmental Engineering, the University of Colorado at Boulder, 262p.
- Bathurst, R. J. (1993). “Investigation of footing restraint on stability of large-scale reinforced soil wall tests”. *Proc., 46<sup>th</sup> Canadian Geotechnical Conference*, 389–398.
- Desrues, J. (1991). “An introduction to strain localization in granular media”. *Physics of Granular Media—Proc., Winter School Les Houches*, 127–142.
- Karpurapu, R. G., and Bathurst, R. J. (1995). “Behavior of geosynthetic reinforced soil retaining walls using the finite element method”. *Computers and Geotechnics*, 17(3), 279–299.
- Lade, P. V., and Jakobsen, K. P. (2002). “Incrementalization of a single hardening constitutive model for frictional materials”. *International Journal for Numerical and Analytical Methods in Geomechanics*, 26(7), 647-659.
- Leshchinsky, D. (2001). “Design dilemma: Use peak or residual strength of soil”. *Geotextiles and Geomembranes*, 19(2), 111-125.
- Suzuki, K., and Yamada, T. (2006). “Double strain softening and diagonally crossing shear bands of sand in drained triaxial tests”. *International Journal of Geomechanics*, 6(6), 440-446.
- Yang, K.-H. (2009). “Stress distribution within geosynthetic-reinforced soil structures”, PhD dissertation, Department of Civil, Architectural, and Environmental Engineering, the University of Texas, Austin, 321p.
- Yoshida, T., and Tatsuoka, F. (1997). “Deformation property of shear band in sand subjected to plane strain compression and its relation to particle characteristics”. *Proc., 14<sup>th</sup> Int. Conference on Soil Mechanics and Foundation Engineering*. Hamburg, Balkema, Rotterdam, 237-240.
- Yoshida, T., Tatsuoka, F., Siddiquee, M., and Kamegai, Y. (1993). “Shear banding in sands in plane strain compression”. *Proc., 3<sup>rd</sup> Int. Workshop on Localization and Bifurcation Theory for Soils and Rocks*, Grenoble, France, 165–179.
- Zornberg, J. G. (2002). “Peak versus residual shear strength in geosynthetic-reinforced soil design”. *Geosynthetics International*, 9(4), 301-318.
- Zornberg, J. G., and Leshchinsky, D. (2001). “Comparison of international design criteria for geosynthetic-reinforced soil structures”. *Geosynthetics and Earth Reinforcement*, ISSMGE-TC9, 106-117.